Flame front speed and onset of instability in the burning of inclined thin solid fuel samples

Bruna Comas and Toni Pujol
Universitat de Girona, 17071 Girona, Spain
(Received 4 October 2013; published 30 December 2013)

We focus on the front propagation of diffusive flames obtained from the downward burning of inclined thermally thin solid fuels. This process consists of a pyrolysis reaction in the solid-phase and a combustion reaction in the gas phase. The solid-phase model is based on two coupled one-dimensional equations of temperature and solid density. We reduce the system into a single one-dimensional equation from which we obtain an analytical expression for the flame front speed. This expression may be understood as an upper bound of the burning spread rate in inclined samples. The gas-phase model is based on four coupled two-dimensional equations. These are employed to derive a criterion for determining the critical inclination angle beyond which the flame behavior becomes unstable. The comparison with the experiments confirms the validity of our predictions.

DOI: 10.1103/PhysRevE.88.063019 PACS number(s): 47.70.Pq, 47.70.Fw, 47.20.−k, 82.33.Vx

I. INTRODUCTION

Combustion is an exothermic process of chemically reacting flows that may produce either a premixed or a nonpremixed flame [1]. Premixed flames occur when both fuel and oxidizer are mixed before burning. In laminar flows of flat premixed gaseous flames, several methods applied to the one-dimensional reaction-convection-diffusion equations that correspond to the conservation equations of mass and energy lead to analytical approximations of the flame front speed [2–4].

On the other hand, diffusion (or, equivalently, nonpremixed) laminar flames arise when the mixing and burning occur simultaneously, like in the downward burning of a cellulosic type sample. In contrast with flat premixed gaseous flames, the combustion of thin solid fuels is, at least, a two-dimensional process, since it involves the mass flux of volatiles at the solid surface and the combustion reaction at the flame height. For such a process, analytical expressions for the speed of the flame front V_f have been obtained after reducing complex two-dimensional reaction-convection-diffusion equations into a single one-dimensional one [5,6]. Although some of these approximations successfully predict the downward flame speed, they fail to explain the burning spread rate over inclined samples where flame instabilities may arise [7].

In this work, we use the solid-phase equations in Sec. III to derive an analytical expression of the upper bound of the flame spread rate. This expression generalizes previous equations and it is valid for inclined surfaces. In Sec. IV we use the gas phase equations to obtain stationary solutions that allow us to calculate the Nusselt number at first-order approximation (equivalent to assume only the gravity component parallel to the surface) and at second-order approximation (equivalent to assume the gravity component normal to the surface). A given value of the ratio of these Nusselt numbers will provide an instability threshold when comparing with experimental data as shown in Sec. V. Here, our approach differs from Refs. [8,9] since it is based on the fundamental governing equations.

II. EXPERIMENTAL SETUP

The experiments were carried out in a combustion chamber, using a controlled atmosphere of 10^5 Pa with a mixture of O_2 and N_2. Figure 1 shows a schematic view of the experimental design. The combustion chamber could be inclined at the angle required for the test.

Cellulosic samples of half-thickness 0.0933 mm and surface density 0.0431 kg m^{-1} were used. The length and width of the samples were 24 × 4 cm, long enough to ensure steady spread and wide enough to minimize effects of lateral heat losses. More details about the samples and justification of the sizes can be found in Ref. [10].

Samples were dried for 2 h at 100 °C and stored for a minimum of 24 h before each experiment. Then they were held by aluminium holders, 2 mm thick and 40 mm wide, in the middle of the chamber; the chamber was closed and inclined to the desired angle. A vacuum was created inside the chamber and then it was filled with O_2 and N_2 at the desired concentration. Gases were mixed during three minutes with a fan and then they were left at rest for 2 min. Samples were ignited uniformly at the top with a coiled nichrome wire. Three repetitions with the same sample configuration and atmospheric concentration were done.

Every experiment was recorded with a high-definition camera at 50 Hz. Videos were later analyzed frame by frame to determine the position of the flame front and the existence (if observed) of an erratic flame behavior that may cause instabilities and produce a substantial variability of the flame front speed once the experiment is repeated under the same conditions. A typical image of the experiment can be seen in Fig. 2. Flame spread velocities were obtained through lineal regression of the front position with respect to time, with a correlation factor of 0.996 or better for all cases.

III. FLAME SPREAD RATE

The combustion of a vertical cellulosic-type sample ignited at the top produces a flame front that propagates downwards at a given speed V_f. For thermally thin solids, many authors have proposed analytical expressions for calculating V_f based either on an energy balance of the solid phase [11] or on an energy balance of the gas phase [6]. Here, we generalize the broadly accepted model of de Ris [12] based on the solid phase equations in order to study the flame spread rate of inclined samples. This model assumes unit Lewis number

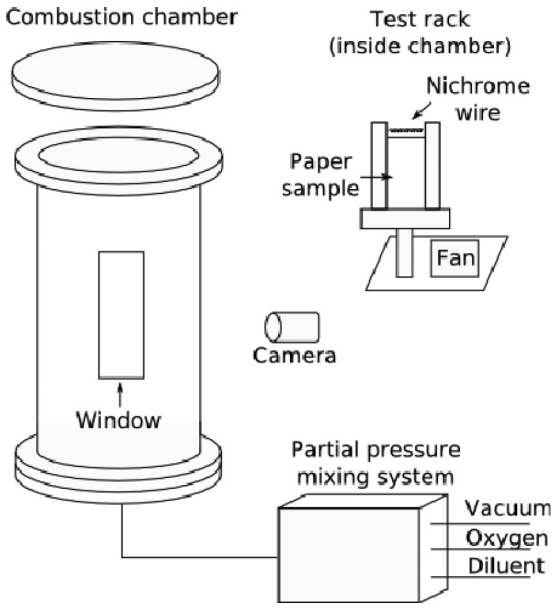

FIG. 1. Schema of the combustion chamber.

(equal thermal and mass diffusivities) and constant transport coefficients.

The burning process of cellulose consists of two main chemical reactions. The first is the endothermic pyrolysis reaction in the solid phase that releases fuel volatiles. The second is the exothermic combustion reaction in the gas phase (oxygen and fuel volatiles) that produces a diffusive flame. The transfer of heat from the flame to the virgin solid ahead preheats the sample, produces the pyrolysis, and sustains the propagation of the flame front.

The governing equations for the solid phase temperature T_s and solid phase density ρ_s are

$$c_s\rho_s\frac{dT_s}{dt} = -\overrightarrow{\nabla}\cdot\overrightarrow{J_s} - \frac{d\rho_s}{dt}[L_v + (c_s - c_g)(T_s - T_\infty)], \quad (1)$$

$$\frac{d\rho_s}{dt} = -A\rho_s e^{-E_s/(RT_s)}, \quad (2)$$

where c_s and λ_s, used in the conductive heat flux term, are the specific heat and conductivity of the solid, L_v is the heat of vaporization, c_g is the gas specific heat, and T_∞ is the room temperature. The term $\overrightarrow{J_s}$ in Eq. (1) includes radiative as well as conductive heat fluxes. In Eq. (2), E_s and A are the activation energy and the preexponential term of the pyrolysis reaction, respectively, with R the universal gas constant.

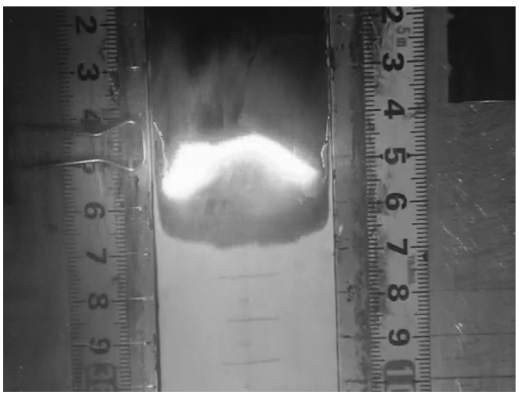

FIG. 2. Image from one experiment made at 30% of O_2, with an inclination of 70° with respect to the horizontal.

By applying the classical analysis of Benguria and collaborators [2] to the set of Eqs. (1) and (2), Ref. [13] obtained an upper bound of the flame front speed,

$$V_f < V_{f,\text{de Ris}} - 2\int_0^1 2\sqrt{F\theta_s}d\theta_s, \quad (3)$$

where

$$F = \frac{\alpha_s T_v A\rho_s e^{-E_s/(RT_s)}[L_v + (c_s - c_g)(T_v - T_\infty)\theta_s]d}{c_s^2\rho_{s\infty}^2(T_v - T_\infty)^2}, \quad (4)$$

with α_s the solid thermal diffusivity, T_∞ and T_v the room and the vaporization temperatures, respectively, θ_s a dimensionless variable defined as

$$\theta_s = \frac{(T_s - T_\infty)}{(T_v - T_\infty)}, \quad (5)$$

and d a function of θ_s such as $d = 0$ at $\theta_s = 1$ and $d = 1$ at $\theta_s = 0$.

In Eq. (3), the term

$$V_{f,\text{de Ris}} = \frac{2\lambda_g(T_{f,\text{ad}} - T_v)}{\tau c_s\rho_{s\infty}(T_v - T_\infty)} \quad (6)$$

corresponds to the de Ris equation with τ the solid thickness, λ_g the gas phase conductivity, and $T_{f,\text{ad}}$ the adiabatic flame temperature (excluding a $\pi/4$ multiplying factor that arises after solving the gas-phase equations).

Equation (3) applies only to the downward combustion of vertical samples. In this configuration, the background convective flow induced by density variations through the flame region opposes the direction of propagation of the flame front. However, as the angle of inclination of the sample increases, the convective flow parallel to the sample decreases in intensity and, therefore, the velocity of the flame front increases. Here, we develop an analytical expression that aims to include this effect.

According to Ref. [14], our model assumes no pyrolysis (constant solid density) ahead of the flame front. Then, in a coordinate system attached to the flame front, Eq. (1) applied to the preheated region (negative x') reduces to

$$c_s\rho_s V_f\frac{dT_s}{dx'} = \lambda_s\frac{d^2T_s}{dx'^2} - \frac{\partial J_s}{\partial y}. \quad (7)$$

The integration of Eq. (7) through the sample thickness (from $y = -\tau$ to $y = 0$) and with the dimensionless variables θ_s (5) and $x = x'/L_{gx+}$ with L_{gx+} as the characteristic gas phase thermal length along x (parallel to the solid surface) of the upper side + of the inclined sample leads to

$$V_f\frac{d\theta_s}{dx} = \frac{\alpha_s}{L_{gx+}}\frac{d^2\theta_s}{dx^2} - \frac{L_{gx+}}{\tau c_s\rho_s(T_v - T_{s\infty})}(J_{cv,y=0} - J_{cv,y=-\tau} + J_{rd,y=0} - J_{rd,y=-\tau}), \quad (8)$$

where J_{cv} and J_{rd} are the conductive and radiative heat fluxes on the upper $y = 0$ and lower $y = -\tau$ sides of the inclined sample. In Eq. (8), we have assumed a uniform temperature across the y direction within the paper sample, which agrees with the thin solid fuel case studied.

The conductive flux in the preheated region is commonly expressed in terms of exponentially decaying functions with a maximum value at the flame leading edge ($x = 0$) [14,15]. At this point, we assume the adiabatic flame temperature $T_{f,\mathrm{ad}}$ as the characteristic gas phase temperature and T_v as the characteristic solid temperature. Therefore, the conductive heat flux at the solid surface at $x = 0$ is equal to $\lambda_g(T_{f,\mathrm{ad}} - T_v)/L_{gy}$ with L_{gy} the characteristic thermal length along y. Thus, the upper $J_{cv,y=0}$ and lower $J_{cv,y=-\tau}$ conductive fluxes in the preheated region are

$$J_{cv,y=0} = -\frac{\lambda_g(T_{f,\mathrm{ad}} - T_v)}{L_{gy+}} e^{x},$$
$$J_{cv,y=-\tau} = \frac{\lambda_g(T_{f,\mathrm{ad}} - T_v)}{L_{gy-}} e^{xL_{gx+}/L_{gx-}}, \tag{9}$$

where L_{gy+}, L_{gy-}, and L_{gx-} are the characteristic gas phase thermal lengths along y or x in the upper $+$ or lower $-$ sides of the inclined sample.

The radiative flux emitted by the flame and absorbed at the virgin solid ahead of the flame front is obtained by using a simplified model in which both flame and paper are constant temperature planes that intersect at the flame leading edge. From the above, the integration of the radiative fluxes from $x = -L/L_{gx+}$ to $x = 0$, where L is the length of the paper, gives

$$\int_{-L/L_{gx+}}^{0} (J_{rd,y=0} - J_{rd,y=-\tau})dx = \varepsilon_f a\sigma T_f^4 (F_{s-f}^{+} + F_{s-f}^{-}) \frac{L}{L_{gx+}}, \tag{10}$$

where ε_f is the flame emissivity, a is the absorptivity of the paper, and T_f is the mean flame temperature. As pointed out in Ref. [15], T_f must be lower than the adiabatic value $T_{f,\mathrm{ad}}$ and here is taken as the mean value of the gas-phase temperature obtained in the one-dimensional flame model of Ref. [16]. The view factors from the paper plane to the flame plane are

$$F_{s-f}^{+,-} = \frac{1}{2}\left(1 + \frac{L_f}{L} - \sqrt{1 + \frac{L_f^2}{L^2} - 2\frac{L_f}{L^2}\cos\beta^{+,-}}\right) \tag{11}$$

with β^+ and β^- the angle between the flame plane and the paper plane in the upper and lower sides of the sample, respectively.

The integration of Eq. (8) from $x = -L/L_{gx+}$ to $x = 0$ gives

$$V_{f,g} = \frac{\alpha_s}{L_{gx+}} \frac{d\theta_s}{dx}\bigg|_{x=0} + \frac{2\alpha_s}{\tau} \frac{\lambda_g(T_{f,\mathrm{ad}} - T_v)}{\lambda_s(T_v - T_{s\infty})} \times \left[\frac{L_{gx+}}{L_{gy+}}(1 - e^{-L/L_{gx+}}) + \frac{L_{gx-}}{L_{gy-}}(1 - e^{-L/L_{gx-}})\right] \times \frac{\alpha_s}{\tau} \frac{\varepsilon_f a\sigma T_f^4 L}{\lambda_s(T_v - T_{s\infty})}(F_{s-f}^{+} + F_{s-f}^{-}). \tag{12}$$

Note that Eq. (12) for the case with no radiation and no conduction through the solid phase reduces to the classical de Ris Eq. (6) for $L_{gx+} = L_{gx-} = L_{gy+} = L_{gy-}$ and $L = \infty$ as it should. Also note that for our radiative calculation, the temperature of the virgin solid is assumed constant and equal to that for the room. This implies no net radiative losses that would tend to lower the velocity in Eq. (12). Therefore, Eq. (12) will overestimate the flame front speed and may be understood as an upper bound to the actual value. This is confirmed by comparison with the experiments as we show in Sec. V.

IV. INSTABILITY

The momentum and continuity gas phase equations for a steady diffusion laminar flame upon an inclined angle ϕ from the vertical are the starting point of the instability analysis. The classical analysis of these equations ignores the gravity component normal to the surface [17–19], either by considering only vertical combustion or low-enough inclination angles ϕ. Our analysis aims to find the critical point where instability arises, and since it is located at angles near $\pi/2$, we must maintain the gravity component normal to the surface. This implies a nontrivial equation for the normal momentum that cannot be solved analytically.

In this section the flame plane is modelled parallel to the surface of the paper ($\beta^+ = \beta^- = 180^\circ$ in Eq. (11)) in order to use Boussinesq approximation for the density. We note that the flame speed Eq. (12) decreases by less than 4% only when varying the β angles from 140° to 180° for the 30% oxygen concentration case. We have experimentally seen with the aid of lateral mirrors inside the combustion chamber that the flame plane does not substantially deviate from the surface until the angle is close to the horizontal, where the flame becomes unstable.

Continuity, momentum, and energy equations will be

$$\frac{\partial(\rho u)}{\partial x} + \frac{\partial(\rho v)}{\partial y} = 0, \tag{13}$$

$$u\frac{\partial u}{\partial x} + v\frac{\partial u}{\partial y} = \nu\frac{\partial^2 u}{\partial y^2} + g\cos\phi\frac{(\rho_\infty - \rho)}{\rho}, \tag{14}$$

$$u\frac{\partial v}{\partial x} + v\frac{\partial v}{\partial y} = \nu\frac{\partial^2 v}{\partial y^2} + g\sin\phi\frac{(\rho_\infty - \rho)}{\rho}, \tag{15}$$

$$u\frac{\partial(T - T_\infty)}{\partial x} + v\frac{\partial(T - T_\infty)}{\partial y} = \alpha\nabla^2(T - T_\infty), \tag{16}$$

where boundary-layer assumptions have been made [17,18,20]. In the above equations we have supposed constant transport properties, unit Lewis number, and velocities much less than the speed of sound. Equations (13), (14), (15), and (16) provide the starting point of a natural convection flux. From these equations we can reach the equations in integral form,

$$\nu\frac{\partial^2 u}{\partial y^2}\bigg]_0^\delta + g\cos\phi\frac{\rho_\infty - \rho}{\rho}\bigg]_0^\delta - g\sin\phi\int_0^\delta \frac{\partial}{\partial x}\left(\frac{\rho_\infty - \rho}{\rho}\right)dy = 0, \tag{17}$$

$$\frac{\partial}{\partial x}\int_0^\delta u(T - T_\infty)dy - \alpha\frac{\partial(T - T_\infty)}{\partial y}\bigg]_0^\delta = 0. \tag{18}$$

The detailed analysis from Eqs. (13), (14), and (15) to the equations in integral form is not given here for the sake of brevity and may be found in the literature [17,21]. For a downward (or inclined) spreading flame, the reference frame

is defined as traveling at the steady flame spread rate V_f. The boundary conditions of the fluid will be

$$\left.\begin{aligned} u &= V_f \\ \rho &= \rho_f \\ T &= T_f \end{aligned}\right\} \quad \text{for} \quad y = 0, \tag{19}$$

$$\left.\begin{aligned} u &= V_f \\ T &= T_\infty \\ \rho &= \rho_\infty \\ \tfrac{\partial u}{\partial y}, \tfrac{\partial (T-T_\infty)}{\partial y}, \tfrac{\partial [(\rho_\infty - \rho)/\rho]}{\partial y} &= 0 \end{aligned}\right\} \quad \text{for} \quad y = \delta. \tag{20}$$

The assumed velocity profile is similar to the velocity profile obtained in the numerical model of Ref. [22],

$$u = u_1 \frac{y}{\delta}\left(1 - \frac{y}{\delta}\right)^2 + V_f, \tag{21}$$

where δ is the thickness of the boundary layer. The density profile is normalized from 1 to 0,

$$\frac{(\rho_\infty - \rho)\rho_f}{(\rho_\infty - \rho_f)\rho} = \left(1 - \frac{y}{\delta}\right)^2. \tag{22}$$

Setting these profiles in the integral equations (17) and (18) gives a set of differential equations that in dimensionless form are

$$\frac{6u_1'}{\delta'^2} = \mathrm{PrGrcos}\phi + \frac{1}{3}\sin\phi \mathrm{PrGr}\frac{d\delta'}{dx'}, \tag{23}$$

$$\frac{1}{30}\frac{d}{dx'}(u_1'\delta' \mathrm{Gr}) = 2\frac{\mathrm{Gr}}{\delta'}, \tag{24}$$

where the dimensionless quantities are $u_1' = u_1 L/\alpha, \delta' = \delta/L$, $x' = x/L$, with L being a characteristic length scale. The Grashof and Prandtl numbers are defined as follows:

$$\mathrm{Gr} = g\frac{\rho_\infty - \rho_f}{\rho *}\frac{L_f^3}{\nu *^2}, \tag{25}$$

$$\mathrm{Pr} = \frac{\nu *}{\alpha *}, \tag{26}$$

where the superscript * means that properties are evaluated at the reference temperature. The set of dimensionless equations (23) and (24) might be solved for an inclined plate first neglecting the term with $d\delta'/dx$ from both equations. This is equivalent to consider only the gravity component parallel to the surface. This first approximation gives

$$\delta_1' = \left(\frac{480}{\mathrm{PrGrcos}\phi}\right)^{1/4} x'^{1/4}, \tag{27}$$

$$u_{1,1}' = \left(\frac{40}{3}\right)^{1/2} (\mathrm{PrGrcos}\phi)^{1/2} x'^{1/2}, \tag{28}$$

The Nusselt number is the ratio of the heat transfer convected by the heat transfer conducted. For natural convection, it is a function of Prandtl and Grashof numbers [20]. It may be expressed as $\mathrm{Nu} = 2/\delta'$ [17]. Then

$$\mathrm{Nu}_1 = \frac{2}{480^{1/4}}(\mathrm{PrGrcos}\phi)^{1/4}. \tag{29}$$

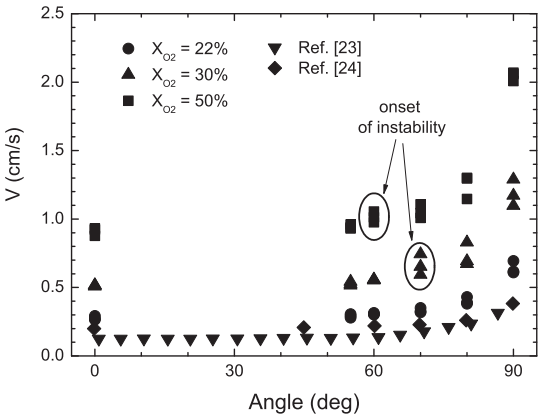

FIG. 3. Flame spread rate versus angle to vertical of the samples.

Taking into account the gravity component normal to the surface allows us to make a second approximation,

$$\delta_2' = \delta_1' \frac{\left[1 - \frac{1}{6}\tan\phi\left(\frac{480}{\mathrm{PrGr}x'}\right)^{1/4}\right]^{1/2}}{1 - \frac{1}{3}\tan\phi\left(\frac{480}{\mathrm{PrGr}x'}\right)^{1/4}}, \tag{30}$$

$$u_{1,2}' = u_{1,1}' + \frac{10^{3/4}}{3^{5/4}}\tan\phi\left(\frac{\mathrm{PrGrcos}\phi}{x'}\right)^{1/4} \times \frac{1 - \frac{1}{6}\tan\phi\left(\frac{480}{\mathrm{PrGr}x'}\right)^{1/4}}{\left[1 - \frac{1}{3}\tan\phi\left(\frac{480}{\mathrm{PrGr}x'}\right)^{1/4}\right]^2}, \tag{31}$$

where the second approximation to the Nusselt number gives

$$\mathrm{Nu}_2 = \mathrm{Nu}_1 \frac{1 - \frac{1}{3}\tan\phi\left(\frac{480}{\mathrm{PrGr}}\right)^{1/4}}{\left[1 - \frac{1}{6}\tan\phi\left(\frac{480}{\mathrm{PrGr}}\right)^{1/4}\right]^{1/2}}. \tag{32}$$

V. RESULTS

Figure 3 shows the experimental results of the flame spread rate as a function of the angle of inclination of the sample for (a) different values of room oxygen concentration (new data, three repetitions on every environmental conditions) and (b) ambient conditions obtained by Refs. [23] and [24]. In Ref. [7] there was also an experimental analysis of the flame front speed for different angles of inclinations but with an external heating supply. In contrast with the results of Kurosaki and coworkers [23,24], Kashiwagi and Newman [7] found that there exists a threshold angle of inclination beyond which the instabilities of the flow lead to large variations on the value of the flame front speed. This critical angle reduces as the value of the external heat supplied to the system increases. This effect is not clearly observed at near-ambient conditions without an external heat supply. However, at higher room oxygen concentration X_{O_2}, we do capture an onset of instability (see Fig. 3) that arises at lower angles of inclination as X_{O_2} increases. Note in Fig. 3 that the flame spread rate is almost constant for a wide range of angles of inclination until a point where the three repetitions of the experiments produce a variation of 20% or higher between flame spread values.

Although such an instability makes it difficult to reproduce the observed flame spread rate by means of an analytical model, a generalization of the de Ris expression (6) in order

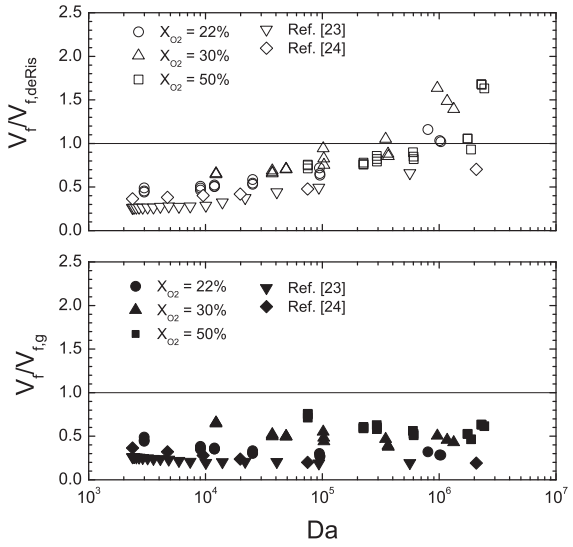

FIG. 4. Normalized values of flame front speed as a function of Damkohler number.

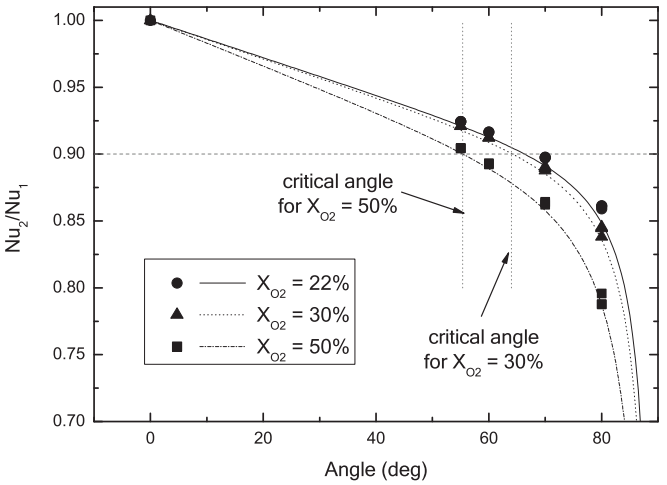

FIG. 5. Nu_2/Nu_1 for all X_{O_2} tested, experimental results, and expected curves.

to predict the trend of data is of great importance, especially at low oxygen concentrations. Figure 4 shows the normalized values of the flame front speeds shown in Fig. 3 as a function of the Damkohler number Da. In Fig. 4, $V_{f,\mathrm{de\,Ris}}$ follows Eq. (6) and $V_{f,g}$ is obtained from Eq. (12) by using the characteristic gas phase thermal lengths as

$$L_{gx+} = \frac{\alpha_g}{V_{\mathrm{acv}} \cos\phi + V_f}, \tag{33}$$

and $L_{gx-} = L_{gy+} = L_{gy-} = L_{gx+}(\phi = 0^\circ)$. In Eq. (33), α_g is the gas-phase thermal diffusivity and V_{acv} is the convective velocity itself, which is calculated as $V_{\mathrm{acv}} = [g\alpha(\rho_\infty - \rho_f)/\rho*]^{1/3}$ (the formula is obtained equating buoyancy and inertia forces [22]). Note that $V_{\mathrm{acv}} \cos\phi$ is the component parallel to the sample surface on the upper side. Below, the paper acts as a barrier for the upward convective flow and, for simplicity, we have employed $L_{gx-} = L_{gy+} = L_{gy-} = L_{gx+}(\phi = 0^\circ)$. The effect of the radiative flux from the flame is taken into account by using a constant value of $\beta^+ = \beta^- = 140^\circ$, although different values of these angles did not produce significant changes on the burning rate, which confirms the small relevance of radiative fluxes in the flame front propagation within the thermal regime [25]. Conduction through the solid in Eq. (12) has been also neglected, since it is not considered of importance in the burning of thin samples [5].

The Damkohler number is the ratio of the residence time for the gas mixture in the flow and the chemical time for the first-order Arrhenius-type reaction [26], being

$$\mathrm{Da} = \frac{\alpha_g}{\rho_g} \frac{Y_F Y_O A_g e^{-E_g/RT_{f,\mathrm{ad}}}}{(V_{\mathrm{acv}} \cos\phi + V_f)^2}, \tag{34}$$

where $A_g (=3.57 \times 10^7\ \mathrm{m^3\ kg^{-1}\ s^{-1}})$ is the preexponential factor, E_g $(=125 \times 10^5\ \mathrm{J\ mol^{-1}})$ is the activation energy, and Y_O and Y_F are the room oxygen and fuel mass fractions, respectively. Following Ref. [26], the fuel mass fraction follows $Y_F = \mathrm{Sc} \ln(1 + B)/B^{0.15}$, where B is the mass transfer number and Sc is the viscous to mass diffusivity ratio. We note that higher values of the Damkohler number are obtained for higher values of inclination angle and/or higher values of room oxygen concentration level (fast reaction).

In Fig. 4, the normalized flame front speed data with respect to the de Ris expression shows a trend to increase as a function of the Damkohler number Da. A similar behavior was already observed in Ref. [26] for the downward ($\phi = 0^\circ$) combustion of thin solid fuels. Our simple analytical model (12) improves the classical one since the normalization of V_f with Eq. (12) tend to be almost independent on Da. However, Eq. (12) overpredicts the flame front speed for a factor of 1.3 to 5, depending on the data and angle employed. In contrast with the classical de Ris expression, however, Eq. (12) behaves as an upper bound whose range of values are even below than those obtained applying Eq. (3) (see Fig. 3 in Ref. [13]).

The onset of the instability can be tracked using the quotient of Nusselt numbers exposed in Sec. IV. Figure 5 shows the ratio of Nusselt numbers calculated as in Eq. (32) for all the situations tested and the theoretical behavior expected. There is a good agreement between the expected curves and experimental values of the quotient of Nusselt numbers; they differ less than 1.5%. The values of $Nu_2/Nu_1 = 0.9$ are chosen as the theoretical critical angle in Fig. 5, being 64.2° and 55.4° for $X_{O_2} = 30\%$ and 50%, respectively. This coincides with the experimental angles showing unstable values seen in Fig. 3. For the $X_{O_2} = 22\%$ case, there is no instability due to the low energy of the flame as also observed in thermally thicker samples [23,24].

The Grashof number is computed using as a reference length the flame length L_f, calculated using the formula obtained in Ref. [11], $L_f \approx 0.0345\{(T_f - T_v)/[(T_v - T_\infty)Y_{O2\infty}]\}^2 \alpha/(V_{\mathrm{acv}} + V_f)$, with the flame spread rate V_f being either the experimental value or the calculated using de Ris's formula [$V_f = (\pi/4)\lambda/(\tau\rho_s c_s)(T_f - T_v)/(T_v - T_\infty)$ [12], i.e., Eq. (12) for $\phi = 0^\circ$ with no radiation neither conduction through the solid phase]. The experimental values of the flame length were not used because of experimental difficulties. The temperature of flame used is the mean of temperatures of the flame zone computed as in Ref. [16]. The reference temperature used for calculating the transport

properties from the gas was the vaporization temperature ($T_v = 640$ K).

For nearly horizontal samples, the experiments show an unstable spread rate that may be triggered by curling of ashes and may be due to the flame in the lower side of the sample, as stated in Ref. [7]. The instability observed can be explained through the importance of the gravity component normal to the surface.

The importance of the normal component of gravity can be traced through the correction done to the Nusselt number Nu_2/Nu_1. After doing the tests, it has been seen that when this correction is greater than 10% of Nu_1, flame spread rates become unstable and expand for a large range of values.

VI. CONCLUSIONS

The flame spread down thermally thin inclined samples is controlled by heat transfer to the unburned part of the sample. For vertical or slightly inclined surfaces, the behavior can be explained using only the component of gravity parallel to the surface. The component of gravity normal to the surface of the sample gains importance as the surface becomes more horizontal and may trigger an instability. In this paper we have generalized the classical analytical expression of the flame front speed [12] in order to be valid for the downward burning of an inclined sample. We have also developed a method to show the importance of the normal component of gravity via the quotient of Nusselt numbers having and not having into account this component. We have found that the instability arises when the correction is greater than a 10%, this being valid for different X_{O_2} concentration values.

ACKNOWLEDGMENTS

B.C. acknowledges the support of a FPU grant from the MICINN. Some data were obtained by Adrià Carmona. We also thank Jordi Vicens and Sergi Saus for their technical assistance. This work has been partially funded by the Generalitat de Catalunya under Grant No. 2009-SGR-374 and the MICINN-FEDER under Grant No. FIS-2012-31307.

[1] D. Drysdale, *An Introduction to Fire Dynamics*, 3rd ed. (Wiley, New York, 2011).
[2] R. D. Benguria, J. Cisternas, and M. C. Depassier, Phys. Rev. E **52**, 4410 (1995).
[3] N. Provatas, T. Ala-Nissila, M. Grant, K. R. Elder, and L. Piche, Phys. Rev. E **51**, 4232 (1995).
[4] T. Pujol, J. Fort, L. Montoro, and J. J. Suñol, Physica A **388**, 4959 (2009).
[5] I. S. Wichman, Prog. Energy Combust. Sci **18**, 553 (1992).
[6] T. Pujol and B. Comas, Phys. Rev. E **84**, 026306 (2011).
[7] T. Kashiwagi and D. L. Newman, Combust. Flame **26**, 163 (1976).
[8] O. Zik, Z. Olami, and E. Moses, Phys. Rev. Lett. **81**, 3868 (1998).
[9] O. Zik and E. Moses, Phys. Rev. E **60**, 518 (1999).
[10] B. Comas and T. Pujol, Combust. Sci. Technol. **184**, 489 (2012).
[11] S. Bhattacharjee, S. Takahashi, K. Wakai, and C. P. Paolini, Proc. Combust. Inst. **33**, 2465 (2011).
[12] J. N. De Ris, in *Proceedings of the Twelfth Symposium (International) on Combustion, University of Poitiers, France, 1968*, edited by The Combustion Institute (The Combustion Institute, Pittsburgh, 1969), p. 241.
[13] T. Pujol and B. Comas, Comb. Sci. Technol. **183**, 1083 (2011).
[14] M. A. Delichatsios, Combust. Flame **135**, 441 (2003).
[15] A. Itoh and Y. Kurosaki, Combust. Flame **60**, 269 (1985).
[16] J. B. Greenberg and P. D. Ronney, Int. J. Heat Mass Transf. **36**, 315 (1993).
[17] J. S. Kim, J. N. de Ris, and K. W. Kroesser, Proc. Comb. Institute **13**, 949 (1971).
[18] K. Annamalai and M. Sibulkin, Combust. Sci. Technol. **19**, 167 (1979).
[19] K. Annamalai and M. Sibulkin, Combust. Sci. Technol. **19**, 185 (1979).
[20] H. Schlichting, *Boundary-Layer Theory*, 7th ed. (McGraw-Hill, New York, 1987).
[21] S. Levy and N. Y. Schenectady, Numer. Heat Transfer, Part A **40**, 841 (2001).
[22] F. C. Duh and C. H. Chen, Combust. Sci. Technol. **77**, 291 (1991).
[23] T. Hirano, S. E. Noreikis, and T. E. Waterman, Combust. Flame **22**, 353 (1974).
[24] M. Sibulkin, W. Ketelhut, and S. Feldman, Combust. Sci. Technol. **9**, 75 (1974).
[25] S. Bhattacharjee, R. Ayala, K. Wakai, and S. Takahashi, Proc. Combust. Inst. **30**, 2279 (2005).
[26] A. C. Fernandez-Pello, S. R. Ray, and I. Glassman, in *Proceedings of the Eighteenth Symposium (International) on Combustion, University of Waterloo, Canada, 1980*, edited by The Combustion Institute (The Combustion Institute, Pittsburgh, 1981), p. 579.